

Diffusion under confinement: hydrodynamic finite-size effects in simulation

Pauline Simonnin^{1,2}, Benoit Noetinger², Carlos Nieto-Draghi², Virginie Marry¹, and Benjamin Rotenberg¹

¹ Sorbonne Universités, UPMC Univ Paris 06, CNRS,

Laboratoire PHENIX, Case 51, 4 Place Jussieu, F-75005 Paris, France and

² IFP Energies Nouvelles, 1 & 4 avenue de Bois-Préau, 92852 Rueil-Malmaison

(Dated: March 16, 2017)

We investigate finite-size effects on diffusion in confined fluids using molecular dynamics simulations and hydrodynamic calculations. Specifically, we consider a Lennard-Jones fluid in slit pores without slip at the interface and show that the use of periodic boundary conditions in the directions along the surfaces results in dramatic finite-size effects, in addition to that of the physically relevant confining length. As in the simulation of bulk fluids, these effects arise from spurious hydrodynamic interactions between periodic images and from the constraint of total momentum conservation. We derive analytical expressions for the correction to the diffusion coefficient in the limits of both elongated and flat systems, which are in excellent agreement with the molecular simulation results except for the narrowest pores, where the discreteness of the fluid particles starts to play a role. The present work implies that the diffusion coefficients for wide nanopores computed using elongated boxes suffer from finite-size artifacts which had not been previously appreciated. In addition, our analytical expression provides the correction to be applied to the simulation results for finite (possibly small) systems. It applies not only to molecular but also to all mesoscopic hydrodynamic simulations, including Lattice-Boltzmann, Multi-Particle Collision Dynamics or Dissipative Particle Dynamics, which are often used to investigate confined soft matter involving colloidal particles and polymers.

The dynamics of fluids can be dramatically modified under confinement down to the molecular scale in nanotubes [1, 2] or nanopores [3], due to the discreteness of matter and to the interfacial fluid-solid interactions. Even in larger pores, wider than tens of molecular sizes which are typical of nanofluidic devices [4, 5] and for which continuum hydrodynamics hold [6], confining walls influence the dynamics of the fluids and solutes [7, 8]. In particular, the diffusion coefficient of particles along a wall is generally reduced due to the friction at the interface.

Quantitatively, the solution of the Stokes equation in a slit pore involves a series of contributions of hydrodynamic images situated inside the solid walls. It predicts a decrease in the diffusion coefficient along the surface with respect to the bulk value, of leading order σ/d , with σ the diameter of the particle and d the distance to the surface [3, 9, 10]. After averaging over the hydrodynamic slab width H , this results in a decrease governed by [12]:

$$D_{\parallel}(H, \infty) \approx D_{\infty} \left[1 + \frac{9}{16} \frac{\sigma}{H} \ln \left(\frac{\sigma}{2H} \right) \right], \quad (1)$$

where ∞ refers to infinite lateral dimensions of the slit on the left-hand side and to the bulk fluid on the right-hand side. Using mode-coupling theory, Bocquet and Barrat obtained a similar scaling, in good agreement with molecular dynamics (MD) simulations, and emphasized its origin as the suppression of long-wavelength modes due to confinement [13]. Slippage at the interface changes the dependence of the diffusion coefficient with distance to the surface [14] and may result in some cases in an average diffusion coefficient larger than the bulk value [1].

MD simulations have generally confirmed the decrease

in the diffusion coefficient near a variety of model and realistic boundaries [16–23] as well as the importance of molecular details in the first adsorbed fluid layers. However, the use of periodic boundary conditions (PBC) in such simulations introduces finite-size effects on the diffusion coefficient, never appreciated under confinement to date, due to the distortion of hydrodynamic flows and the spurious hydrodynamic interaction between periodic images. For bulk fluids in a cubic simulation box, the correction to the diffusion coefficient reads [24–27] $D(L) = D_{\infty} - \xi k_B T / 6\pi\eta L$, with L the box size, k_B Boltzmann’s constant, T the temperature, η the viscosity and $\xi \approx 2.837$. Recently, the effect of the box shape has also been considered for bulk fluids: The components of the diffusion tensor in anisotropic boxes may in some cases be larger than D_{∞} and diverge with system size in the limit of highly elongated boxes [28, 29]. These features can also be explained from hydrodynamics [30–32].

Surprisingly, despite the ever growing importance of simulations to characterize the dynamics of confined fluids, such finite-size effects have not been investigated under confinement. Here we show that the diffusion of confined fluids is not only affected by the confining distance but is also influenced within simulations by finite-size effects due to the use of PBC in the directions parallel to the surfaces. We demonstrate this fact using MD simulations of a simple fluid confined inside a slit pore. We show that the diffusion coefficient is generally larger than the value for the unconfined fluid, by a factor which is in fact significant for typical box shapes, thereby illustrating the limitations of previous simulation results. Using continuum hydrodynamics, we further obtain the scaling with system size in the limits of elongated and flat sys-

tems. As in the case of bulk fluids, the present analysis opens the way to systematic extrapolation to the limit of infinite systems (for a fixed confining distance).

We simulate a Lennard-Jones (LJ) fluid under the same conditions as in previous work illustrating finite-size effects in bulk fluids [26, 30], namely a reduced density $\rho^* = \rho\sigma^3 = 0.7$ and reduced temperature $T^* = k_B T/\epsilon = 2.75$ with σ and ϵ the LJ diameter and energy, respectively. The fluid is confined between rigid planar surfaces consisting of a square lattice with a spacing of 1σ . The fluid-surface interactions are characterized by a diameter $\sigma_{FS} = \sigma$ and an energy ϵ_{FS} equal to ϵ for 3/4 of the wall atoms and 3ϵ for the remaining 1/4 (see the square lattice in Figure 1). This pattern ensures the absence of slippage at the wall, as demonstrated by the velocity profile under shear (with a wall velocity of $v_{wall} = \pm 0.5$ LJ units) in Figure 1. The distance between the LJ walls is $H + 2\sigma$, with H the distance between the shear planes on both surfaces, while the size of the simulation box L is the same in the other two directions. In order to assess the finite-size effects due to both the PBC and the confinement, we consider systems with L between 6 and 80σ and H ranging from 10 to 160σ , corresponding to particle numbers from 587 to 30720.

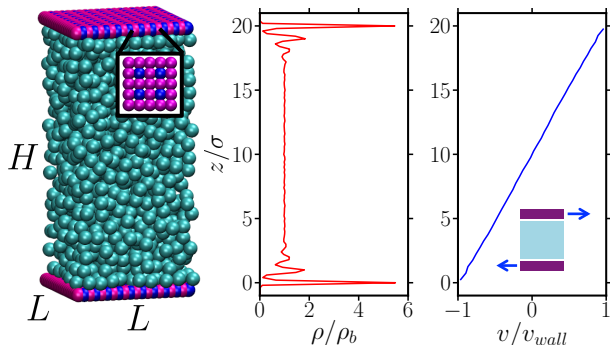


FIG. 1. The simulated systems consists of a LJ fluid between rigid LJ walls. The wall atoms are placed on a square lattice, with every fourth atom interacting three times more strongly with the fluid than the others. In addition to the effect of the confining distance, we investigate the influence of periodic boundary conditions by varying the size $L_x = L_y = L$ of the simulation box in the directions along the surfaces. $L_z = H$ indicates the distance between the first adsorbed fluid layers on both surfaces (the distance between the walls is $H + 2\sigma$), as shown in the central part of the figure for $H = 20\sigma$, which also correspond to the shear planes for such surfaces without slip at the walls, as demonstrated by the velocity profile under shear. We consider both elongated ($H > L$, as shown) and flat ($H < L$) systems.

All MD simulations are performed using the LAMMPS simulation package [33], using a time step of $10^{-3}t^*$, with $t^* = \sigma\sqrt{m/\epsilon}$ and a cut-off distance 2.5σ to compute the LJ interactions. The systems are first equilibrated in the NVT ensemble during $200t^*$, using a Nosé-

Hoover thermostat with a time constant of t^* . After equilibration, trajectories in the NVE ensemble are produced for $4 \cdot 10^4 t^*$ up to $1.6 \cdot 10^5 t^*$ depending on system size, from which diffusion coefficients parallel to the surfaces are computed from the slope of the mean-square displacement (MSD) in the time range $5 \cdot 10^3 - 1.5 \cdot 10^4 t^*$ ($4 - 8 \cdot 10^5 t^*$ for $H \geq 80\sigma$ with $L = 6\sigma$). For each system, reported results correspond to averages and standard errors over 16 independent runs.

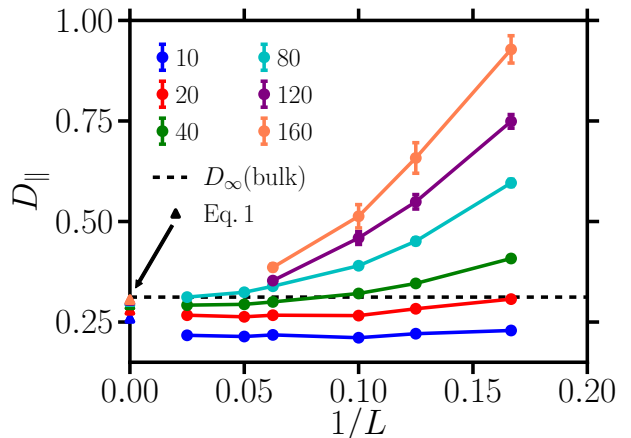


FIG. 2. Diffusion coefficient along the surface D_{\parallel} as a function of the inverse box size parallel to the walls, $1/L$, for the various confining distances H (all in LJ units). The horizontal dashed line indicates the extrapolated value for the bulk fluid in an infinite cubic box, D_{∞} , while the values predicted by hydrodynamics for $L \rightarrow \infty$, Eq. 1, are indicated by triangles on the y axis.

Figure 2 reports the diffusion coefficient parallel to the surfaces D_{\parallel} as a function of $1/L$ (by analogy with the scaling for a cubic box of bulk fluid) for the various confining distances H . This figure also shows the results for an infinite bulk system, equal to $D_{\infty} = 0.312 \pm 0.005$ LJ units in the present case [30], as well as the prediction of Eq. 1 for the limit $L \rightarrow \infty$ under confinement. We first note that the diffusion coefficient increases with H , as expected, and that the results for large L are consistent with Eq. 1 (except for the narrowest pore). However, there is also a dramatic influence of the periodicity along the surface which increases with pore width H . For the smaller L , the diffusion coefficient is larger than D_{∞} for an infinite unconfined fluid. For wide thin pores (large H , small L), it can be several times larger than D_{∞} .

For elongated boxes ($H > L$), the results of Figure 2 seem to suggest a correction to the diffusion coefficient proportional to H/L^2 . Such a scaling in this regime has been predicted on the basis of hydrodynamic arguments by Detcherry and Bocquet, who computed the enhancement of diffusion in nanometric pipes due to the thermal fluctuations of the center of mass of the

fluid [34, 35]. This increase:

$$\Delta D_{\parallel} = D_{\parallel}(H, L) - D_{\parallel}(H, \infty), \quad (2)$$

with $D_{\parallel}(H, \infty)$ given by Eq. 1, is related to the total fluid-wall friction coefficient λ via the Einstein relation $\Delta D_{\parallel} = k_B T / \lambda$. The friction coefficient is then derived from the total force on the walls exerted by the fluid with typical velocity v as $F \sim \lambda v$, which is also proportional to the fluid-wall contact area $2L^2$ and the viscous stress at the boundary $\sim \eta v / H$. Therefore, the increase in the diffusion coefficient scales as $\Delta D_{\parallel} \sim \frac{k_B T}{\eta} \frac{H}{L^2}$. More precisely, they obtained the following result for the present slit geometry :

$$\Delta D_{\parallel} = \mathcal{D}_{c.o.m.} = \frac{1}{12} \frac{k_B T}{\eta} \frac{H}{L^2}, \quad (3)$$

with $\mathcal{D}_{c.o.m.}$ the diffusion coefficient for the center of mass of the fluid. Figure 3 reports the simulation results in a dimensionless form, namely $\Delta D_{\parallel} H \eta / k_B T$ as a function of H/L (here we use the bulk value of the viscosity, $\eta = 1.28$ LJ units [30]). The collapse of the simulation results on a master curve confirms the hydrodynamic origin of the finite-size effects. While Eq. 3 accounts qualitatively for the observed behavior it is not quantitative.

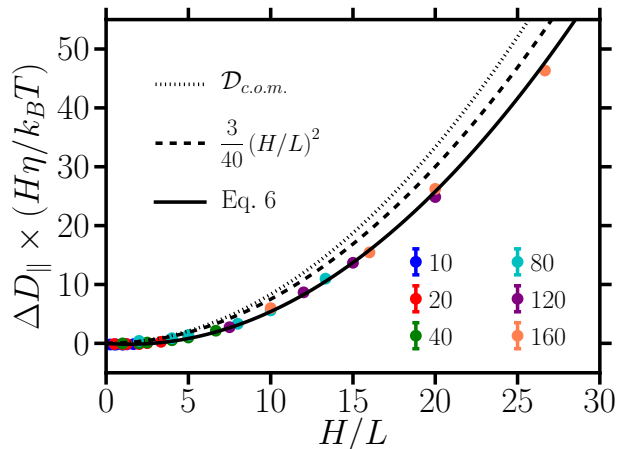


FIG. 3. Finite size correction to the diffusion coefficient along the surface, ΔD_{\parallel} , with respect to Eq. 1 for an infinite slit pore of width H , as a function of H/L with L the size of the periodic system in the directions along the walls. The dotted line corresponds to Eq. 3, *i.e.* the hydrodynamic fluctuations of the center-of-mass; the dashed line indicates the prediction obtained by treating the sum over periodic images (Eq. 40) as an integral, while the solid line is the the full result of Eq. 6 which corrects for the spurious self-interaction introduced by this assumption.

In order to go beyond this simple scaling argument, we now compute the correction to the diffusion coefficient due to both confinement and PBC along the surfaces by

solving the full hydrodynamic problem. Following previous studies of bulk fluids [24, 26, 30], this is achieved by computing the mobility from the solution of the Stokes equation for an incompressible fluid, $\eta \nabla^2 \mathbf{v} - \nabla p + \mathbf{f} = 0$, with \mathbf{v} and p the velocity and pressure fields. In bulk fluids, the force density $\mathbf{f} = \mathbf{F} [\delta(\mathbf{r}) - \frac{1}{V}]$ with \mathbf{F} a force, δ the Dirac distribution and V the volume of the system, includes both a perturbation at $\mathbf{r} = 0$ and a compensating “background force” which enforces the constraint of vanishing total force on the system. This compensating force provides in fact the main contribution to the system-size dependence of the diffusion coefficient.

In the present case, the broken translational invariance in the direction of confinement renders the problem more difficult. The mobility tensor defined by $\mathbf{v}(\mathbf{r}) = \mathbb{T}(\mathbf{r}, \mathbf{r}_0) \cdot \mathbf{F}(\mathbf{r}_0)$, provides the flow at $\mathbf{r} = (x, y, z)$ induced by a force \mathbf{F} applied at $\mathbf{r}_0 = (x_0, y_0, z_0)$ and is related to the diffusion tensor as $\mathbb{T} = \mathbb{D} / k_B T$. The expression of the mobility tensor \mathbb{T}^∞ for the case of an infinite slit pore ($L \rightarrow \infty$) with non-slip boundary conditions at the walls ($\mathbf{v} = 0$ for $z = 0$ and H), previously obtained by Liron and Mochon [2] or Swan and Brady [3], is derived in a convenient form for the present work in the Supplementary Material [12], which also provide the details of the following calculations. It depends on the relative position along the wall $(x - x_0, y - y_0)$ and on both z and z_0 . We note that contrary to the bulk case, the mobility can be obtained in the presence of solid walls even without compensating background. The effect of the latter, which remains necessary to enforce the constraint of total momentum conservation, can be introduced separately by subtracting the average mobility over the pore volume. The average correction to the diffusion tensor then reads $\Delta \mathbb{D} = k_B T [\langle \delta \mathbb{T}^i \rangle - \langle \delta \mathbb{T}^b \rangle]$ where the first term corresponds to the effect of periodic images and the second to that of the compensating background.

The effect of periodic images (mL, nL) along the surfaces can then be expressed in real space as a correction to the mobility $\delta \mathbb{T}^i(x, y, z) = \sum_{(m,n) \neq (0,0)} \mathbb{T}^\infty(x - mL, y - nL, z, z_0 = z)$, with $z_0 = z$ since the images are located in the same plane. We consider here the mobility averaged over the whole pore, which from translational invariance along the surfaces simplifies to:

$$\langle \delta \mathbb{T}^i \rangle = \frac{1}{H} \int_0^H dz \sum_{(m,n) \neq (0,0)} \mathbb{T}^\infty(-mL, -nL, z, z). \quad (4)$$

The average contribution of the background force, summed over all periodic images, can be written as an integral over all space:

$$\langle \delta \mathbb{T}^b \rangle = \frac{1}{H^2} \iint_0^H dz dz_0 \iint_{-\infty}^{\infty} \frac{dx_0 dy_0}{L^2} \mathbb{T}^\infty(-x_0, -y_0, z, z_0). \quad (5)$$

Taking advantage of the symmetry of the system, the component along the surface is computed from $\mathbb{T}_{\parallel} =$

$\frac{1}{2}(\mathbb{T}_{xx} + \mathbb{T}_{yy})$. In addition, the integral over x_0 and y_0 in $\langle \delta \mathbb{T}^b \rangle$ is conveniently computed as the value for $\mathbf{q} = 0$ of the 2D Fourier transform $\hat{\mathbb{T}}_{\parallel}^{\infty}(\mathbf{q}, z, z_0)$. We show in the Supplementary Material [12] that the contribution of the background is equal to $\langle \delta \mathbb{T}_{\parallel}^b \rangle = H/24\eta L^2$.

For elongated systems ($H > L$), the discrete sum over images in Eq. 40 can be estimated by the corresponding integral, which is equal to $7H/60\eta L^2$, after removing the term corresponding to $(m, n) = (0, 0)$, which is given by $-3\ln(1 + \sqrt{2})/4\pi\eta L$ (see [12] for both demonstrations). Subtracting the background, we finally obtain the correction to the diffusion coefficient:

$$\Delta D_{\parallel}(H > L) = \frac{k_B T}{\eta} \left[\frac{3}{40} \frac{H}{L^2} - \frac{3\ln(1 + \sqrt{2})}{4\pi L} \right]. \quad (6)$$

The first term is consistent with the scaling argument of Detchevy and Bocquet (see Eq. 3) and the curvature is only 10% smaller. As shown in Figure 3, it is closer to the simulation results, but the second $\mathcal{O}(1/L)$ term, which corrects for the spurious self-interaction introduced upon replacing the discrete sum by an integral, is necessary to describe the simulation results quantitatively. The agreement of Eq. 6 with the latter is excellent. This confirms the hydrodynamic origin of the observed finite-size effects due to the PBC, in addition to the effect of confinement correctly described by Eq. 1 for sufficiently wide pores.

In the opposite regime of flat simulation boxes ($H < L$), the mobility \mathbb{T}^{∞} decays exponentially due to the screening of hydrodynamic interactions by the walls [12]. Therefore the sum (Eq. 40) becomes negligible compared to the effect of the background (Eq. 5), so that:

$$\Delta D_{\parallel}(H < L) \approx -\frac{1}{24} \frac{k_B T}{\eta} \frac{H}{L^2}. \quad (7)$$

This explains the decrease in the diffusion coefficient with $1/L$ observed for the narrower pores in Figure 2. Eq. 7 is in very good agreement with the results for $H = 20\sigma$ (within 5%) and 40σ (within 1%), but still overestimates the diffusion coefficient for $H = 10\sigma$ (by $\sim 25\%$). Since the fluid is perturbed by the surfaces over 2-3 layers on each wall (see the density profile in Figure 1), it is not surprising that the present continuum hydrodynamics calculations, which neglect molecular effects, are not quantitative in this case.

Vögele and Hummer recently obtained analytical expressions for the correction to the diffusion tensor for bulk fluids in anisotropic boxes [32], in good agreement with numerical and molecular simulation results [30]. For elongated systems, the correction for the component corresponding to D_{\parallel} scales as $\frac{k_B T}{\eta} [H/12L^2 - \xi_1/L]$, with $\xi_1 \approx 0.23$, *i.e.* the same functional form as Eq. 6 but with different numerical factors. In contrast, for flat systems the scaling goes as $\frac{k_B T}{\eta} [\ln(L/H)/4\pi H - \xi_2/H]$,

with $\xi_2 \approx 0.15$ and therefore diverges as $L \rightarrow \infty$, which is of course not the case under confinement. Therefore, despite some similarities, the present case of confined fluids is fundamentally different due to the boundary conditions at the solid-liquid interface. We finally note that, as for bulk fluids, the role of the background force enforcing the constraint of total momentum conservation is essential. In the bulk, the correction corresponding to the minimum-image cell accounts for $\approx 85\%$ of the total correction [26]. Under confinement, the total background contribution represents a large part of the $\mathcal{O}(H/L^2)$ term in Eq. 6 for elongated systems (the nearest-image cell corresponds to the $\mathcal{O}(1/L)$ term) [12] and almost 100% of the effect for flat systems (Eq. 7).

Ideally, the limit $L \rightarrow \infty$ should be obtained from simulations with $L \gg H$ in order to minimize the finite-size effects due to PBC (see Figure 2). The only exception is that of confinement down to the molecular scale, where such finite-size effects are less dramatic (see *e.g.* Ref. 37) due to the discreteness of the fluid and the predominance of interfacial features. However, in practice typical boxes are rather elongated or cubic ($L \leq H$) than flat, because the latter regime is computationally more expensive. The present work suggests that it is possible to minimize the finite-size effects in the other limit of elongated boxes by choosing an aspect ratio of $H/L = 10 \ln(1 + \sqrt{2})/\pi \approx 2.8$ for which ΔD_{\parallel} cancels (see Eq. 6). It further demonstrates the hydrodynamic origin of these effects on the diffusion coefficient, as for bulk fluids, and offers with Eq. 6 an estimate of the correction to be applied to the simulation results for finite (possibly small) systems.

The present work not only applies to molecular simulations, but also to all mesoscopic hydrodynamic simulations, including Lattice-Boltzmann, Multi-Particle Collision Dynamics or Dissipative Particle Dynamics. Therefore the effects of PBC should also be taken into account in the study of confined soft matter involving colloidal particles and polymers. The analysis could also be extended to other geometries such as nanotubes, as well as to slip boundary conditions at the interface, since slippage is known to have an influence on the diffusion coefficient [1, 14]. In both cases, the same strategy can be applied using the corresponding mobility tensor for the limit of an infinite system along the surfaces.

-
- [1] A. Striolo, Nano Letters **6**, 633 (2006).
 - [2] K. Falk, F. Sedlmeier, L. Joly, R. R. Netz, and L. Bocquet, Nano Letters **10**, 4067 (2010).
 - [3] K. Falk, B. Coasne, R. Pellenq, F.-J. Ulm, and L. Bocquet, Nature Communications **6** (2015).
 - [4] K. Mathwig, D. Mampallil, S. Kang, and S. G. Lemay, Physical Review Letters **109**, 118302 (2012).
 - [5] A. Siria, P. Poncharal, A.-L. Biance, R. Fulcrand, X. Blase, S. T. Purcell, and L. Bocquet, Nature **494**, 455

- (2013).
- [6] L. Bocquet and E. Charlaix, *Chemical Society Reviews* **39**, 1073 (2010).
- [7] M. H. J. Hagen, I. Pagonabarraga, C. P. Lowe, and D. Frenkel, *Physical review letters* **78**, 3785 (1997).
- [8] K. Huang and I. Szlufarska, *Nature Communications* **6**, 8558 (2015).
- [9] H. Faxén, *Annalen der Physik* **373**, 89 (1922).
- [10] J. R. Blake and A. T. Chwang, *Journal of Engineering Mathematics* **8**, 23 (1974).
- [3] J. W. Swan and J. F. Brady, *Physics of Fluids* (1994-present) **22**, 103301 (2010).
- [12] *See supplemental material at [url will be inserted by publisher] for the derivation of eq. 1, of the mobility tensor under confinement in an infinite slit pore, and of the correction to the diffusion coefficient due to periodic boundary conditions (eqs. 6 and 7).*
- [13] L. Bocquet and J.-L. Barrat, *EPL (Europhysics Letters)* **31**, 455 (1995).
- [14] E. Lauga and T. M. Squires, *Physics of Fluids* (1994-present) **17**, 103102 (2005).
- [1] A. Saugey, L. Joly, C. Ybert, J. L. Barrat, and L. Bocquet, *Journal of Physics: Condensed Matter* **17**, S4075 (2005).
- [16] P. Liu, E. Harder, and B. J. Berne, *The Journal of Physical Chemistry B* **108**, 6595 (2004).
- [17] V. Marry, B. Rotenberg, and P. Turq, *Phys. Chem. Chem. Phys.* **10**, 4802 (2008).
- [18] C. Sendner, D. Horinek, L. Bocquet, and R. R. Netz, *Langmuir* **25**, 10768 (2009).
- [19] A. Botan, B. Rotenberg, V. Marry, P. Turq, and B. Noetinger, *The Journal of Physical Chemistry C* **115**, 16109 (2011).
- [20] M.-J. Wei, L. Zhang, L. Lu, Y. Zhu, K. E. Gubbins, and X. Lu, *Physical Chemistry Chemical Physics* **14**, 16536 (2012).
- [21] H. Hoang and G. Galliero, *The Journal of Chemical Physics* **136**, 184702 (2012).
- [22] B. Siboulet, J. Molina, B. Coasne, P. Turq, and J.-F. Dufreche, *Molecular Physics* **111**, 3410 (2013).
- [23] Y. von Hansen, S. Gekle, and R. R. Netz, *Physical Review Letters* **111**, 118103 (2013).
- [24] B. Dünweg and K. Kremer, *The Journal of chemical physics* **99**, 6983 (1993).
- [25] M. Fushiki, *Physical Review E* **68**, 021203 (2003).
- [26] I.-C. Yeh and G. Hummer, *The Journal of Physical Chemistry B* **108**, 15873 (2004).
- [27] S. Tazi, A. Botan, M. Salanne, V. Marry, P. Turq, and B. Rotenberg, *Journal of Physics: Condensed Matter* **24**, 284117 (2012).
- [28] D. Rozmanov and P. G. Kusalik, *The Journal of Chemical Physics* **136**, 044507 (2012).
- [29] G. Kikugawa, S. Ando, J. Suzuki, Y. Naruke, T. Nakano, and T. Ohara, *The Journal of chemical physics* **142**, 024503 (2015).
- [30] A. Botan, V. Marry, and B. Rotenberg, *Molecular Physics* **113**, 2674 (2015).
- [31] G. Kikugawa, T. Nakano, and T. Ohara, *The Journal of Chemical Physics* **143**, 024507 (2015).
- [32] M. Vögele and G. Hummer, *The Journal of Physical Chemistry B* **120**, 8722 (2016).
- [33] LAMMPS, , <http://lammmps.sandia.gov>.
- [34] F. Detcheverry and L. Bocquet, *Physical Review Letters* **109**, 024501 (2012).
- [35] F. Detcheverry and L. Bocquet, *Physical Review E* **88**, 012106 (2013).
- [2] N. Liron and S. Mochon, *Journal of Engineering Mathematics* **10**, 287 (1975).
- [37] M. Holmboe and I. C. Bourg, *The Journal of Physical Chemistry C* **118**, 1001 (2014).

The authors are grateful to Lydéric Bocquet and Jean-Pierre Hansen for useful discussions. They acknowledge financial support from IFPEN and access to computing resources on Curie (TGCC, French National HPC) via the GENCI project x2016087684 and on MeSU (UPMC).

Supplementary Material

I. Confined diffusion for an infinite slit pore

Here we explain the expression for the hydrodynamic correction to the diffusion due to the confinement, for an infinite slit pore (Eq. 1) of the main text. We simply express the results of Saugey *et al.* [1] with the notations of the present work. The local diffusivity at position z within the pore, defined here by the position of the hydrodynamic shear planes at $z = \pm H/2$, is assumed to result from the combined frictions due to the two walls. For the case of non-slip boundary conditions considered in the present work, this reads:

$$D_{\parallel}(z) = \frac{D_{\infty}}{\frac{1}{1 - \frac{9}{16} \frac{\sigma}{2z + \sigma}} + \frac{1}{1 - \frac{9}{16} \frac{\sigma}{2(H-z) + \sigma}} - 1} \quad (8)$$

with D_{∞} the diffusion coefficient of the unconfined fluid and σ the particle diameter. Averaging over the pore width, we obtain:

$$\begin{aligned} \frac{\langle D_{\parallel} \rangle}{D_{\infty}} &= \frac{1}{H} \int_0^H \frac{D_{\parallel}(z)}{D_{\infty}} dz \\ &= 1 - \frac{9\sigma}{8H} \sqrt{\frac{7\sigma + 16H}{25\sigma + 16H}} \operatorname{Argh}\left(\frac{16H}{\sqrt{(7\sigma + 16H)(25\sigma + 16H)}}\right) \end{aligned} \quad (9)$$

For wide pores ($H \gg \sigma$) this is approximately given by $\approx 1 + \frac{9}{16} \frac{\sigma}{H} \ln\left(\frac{\sigma}{2H}\right)$, which corresponds to Eq. 1 of the main text.

II. Mobility tensor for an infinite slit pore

In the main text we use the mobility tensor defined by $\mathbf{v}(\mathbf{r}) = \mathbb{T}^{\infty}(\mathbf{r}, \mathbf{r}_0) \cdot \mathbf{F}(\mathbf{r}_0)$ which provides the fluid velocity $\mathbf{v}(\mathbf{r})$ at position $\mathbf{r} = (x, y, z)$ induced by a force \mathbf{F} applied at $\mathbf{r}_0 = (x_0, y_0, z_0)$, for an infinite slit pore. Here we derive its expression.

Basic hypotheses and equations

We consider the flow of a Newtonian fluid at low Reynolds number. The motion of the fluid confined between two infinite plates $z = \pm H/2$ parallel to the xy plane is governed by the Stokes equation $\eta \nabla^2 \mathbf{v}(\mathbf{r}) + \mathbf{f}(\mathbf{r}) - \nabla p(\mathbf{r}) = \mathbf{0}$, its incompressibility (Eq. 11) and the non-slip boundary conditions at the wall (Eq. 12). Here η denote the viscosity, while $\mathbf{f}(\mathbf{r})$ and $p(\mathbf{r})$ denote a body force field and the associated pressure. The mobility tensor $\mathbb{T}^{\infty}(\mathbf{r}, \mathbf{r}_0)$ is obtained as the solution of the so-called Stokeslet problem:

$$\eta \nabla^2 \mathbf{v}(\mathbf{r}) + \delta(x)\delta(y)\delta(z - z_0)F_{\parallel} \mathbf{e}_x - \nabla p(\mathbf{r}) = \mathbf{0} \quad (10)$$

$$\nabla \cdot \mathbf{v}(\mathbf{r}) = 0 \quad (11)$$

$$\mathbf{v}(\mathbf{r}) = \mathbf{0} \text{ for } z = \pm H/2 \quad (12)$$

with a unit horizontal force density ($F_{\parallel} = 1$) acting without loss of generality at $\mathbf{r}_0 = (0, 0, z_0)$ in the x direction. This problem was fully solved by Liron and Mochon [2]. Their solution involves multiple reflexions at the walls, complex integral representations and series expansion techniques, which render the final form difficult to exploit for the present work. We present here a more direct route, along the lines of Swan and Brady [3].

Solution of the Stokeslet problem under confinement

From the Stokes and incompressibility equations (Eqs. 10 and 11), the pressure obeys:

$$\nabla^2 p(\mathbf{r}) = \delta'(x)\delta(y)\delta(z - z_0)F_{||}. \quad (13)$$

It is convenient to introduce the partial Fourier transform with respect to x and y defined by:

$$h(\mathbf{q}, z) = \iint_{-\infty}^{\infty} dx dy h(x, y, z) e^{iq_x x + iq_y y} \quad (14)$$

with $\mathbf{q} = (q_x, q_y)$. The local velocity may also be decomposed into parallel $\mathbf{v}_{||}(x, y, z)$ and vertical directions $\mathbf{v}_z(x, y, z)$. Using these notations, the Fourier transforms $p(\mathbf{q}, z)$, $\mathbf{v}_{||}(\mathbf{q}, z)$, and $\mathbf{v}_z(\mathbf{q}, z)$ are solutions of:

$$-q^2 p(\mathbf{q}, z) + \frac{\partial^2 p(\mathbf{q}, z)}{\partial z^2} = iq_x \delta(z - z_0) F_{||} \quad (15)$$

$$\eta q^2 \mathbf{v}_{||}(\mathbf{q}, z) - \eta \frac{\partial^2 \mathbf{v}_{||}(\mathbf{q}, z)}{\partial z^2} = F_{||} \delta(z - z_0) \mathbf{e}_x - i\mathbf{q} p(\mathbf{q}, z) \quad (16)$$

$$\eta q^2 v_z(\mathbf{q}, z) - \eta \frac{\partial^2 v_z(\mathbf{q}, z)}{\partial z^2} = \frac{\partial p(\mathbf{q}, z)}{\partial z} \quad (17)$$

$$i\mathbf{q} \cdot \mathbf{v}_{||}(\mathbf{q}, z) + \frac{\partial v_z(\mathbf{q}, z)}{\partial z} = 0 \quad (18)$$

$$\mathbf{v}(\mathbf{q}, z) = 0 \text{ for } z = \pm H/2 \quad (19)$$

These second order differential equations can be solved using standard methods, yielding:

$$\left\{ \begin{array}{l} p(\mathbf{q}, z) = A \cosh(qz) + B \sinh(qz) + \frac{iq_x}{2q} \exp(q|z - z_0|) F_{||} \\ -\eta v_x(\mathbf{q}, z) = A^x \cosh(qz) + B^x \sinh(qz) - \frac{iq_x}{2q} z A \sinh(qz) - \frac{iq_x}{2q} z B \cosh(qz) \\ \quad + \frac{q_x^2}{4q^2} |z - z_0| \exp(q|z - z_0|) F_{||} + \frac{1}{2q} \exp(q|z - z_0|) F_{||} - \frac{q_x^2}{4q^3} \exp(q|z - z_0|) F_{||} \\ -\eta v_y(\mathbf{q}, z) = A^y \cosh(qz) + B^y \sinh(qz) - \frac{iq_y}{2q} z A \sinh(qz) - \frac{iq_y}{2q} z B \cosh(qz) \\ \quad + \frac{q_x q_y}{4q^2} |z - z_0| \exp(q|z - z_0|) F_{||} - \frac{q_x q_y}{4q^3} \exp(q|z - z_0|) F_{||} \\ -\eta v_z(\mathbf{q}, z) = A^z \sinh(qz) + B^z \cosh(qz) - \frac{1}{2} A z \cosh(qz) - \frac{1}{2} B z \cosh(qz) \\ \quad - \frac{iq_x(z - z_0)}{4q} \exp(q|z - z_0|) F_{||} \end{array} \right. \quad (20)$$

where $q = \|\mathbf{q}\|$ and where all the prefactors (to be determined in the following) depend on z_0 . In the following this dependence is dropped for the sake of clarity, but it needs to be included when performing averages over the pore in the next sections. One must manipulate quantities such as $(z - z_0)$ and $|z - z_0|$ with caution, especially when computing derivatives of $\exp(q|z - z_0|)$ with respect to z . The eight constants A, B, A^x, B^x, A^y, B^y and A^z, B^z are determined from the boundary conditions and the divergence-free condition. Differentiating the last equation with respect to z , we obtain:

$$\begin{aligned} -\eta \frac{\partial v_z(\mathbf{q}, z)}{\partial z} &= qA^z \cosh(qz) + qB^z \sinh(qz) - \frac{1}{2} A \cosh(qz) - \frac{1}{2} B \sinh(qz) \\ &\quad - \frac{1}{2} A q z \sinh(qz) - \frac{1}{2} B q z \cosh(qz) \\ &\quad - \frac{iq_x}{4q} \exp(q|z - z_0|) F_{||} - \frac{iq_x |z - z_0|}{4} \exp(q|z - z_0|) F_{||} \end{aligned} \quad (21)$$

Inserting this expression together with v_x and v_y into the incompressibility condition Eq. 18, one obtains the following simple conditions:

$$\left\{ \begin{array}{l} \cosh(qz)(iq_x A^x + iq_y A^y + qA^z - \frac{1}{2} A) = 0 \\ \sinh(qz)(iq_x B^x + iq_y B^y + qB^z - \frac{1}{2} B) = 0 \end{array} \right. \quad (22)$$

Since this holds for every position z , the terms in parentheses must vanish. These conditions can be written in compact form as:

$$\left\{ \begin{array}{l} A = 2i\mathbf{Q} \cdot \mathbf{A} \\ B = 2i\mathbf{Q} \cdot \mathbf{B} \end{array} \right. \quad (23)$$

where we have introduced the following vectors:

$$\mathbf{A} = \begin{pmatrix} A^x \\ A^y \\ A^z \end{pmatrix}; \quad \mathbf{B} = \begin{pmatrix} B^x \\ B^y \\ B^z \end{pmatrix}; \quad \mathbf{Q} = \begin{pmatrix} q_x \\ q_y \\ -iq \end{pmatrix} \quad (24)$$

Inserting these results in Eq 20 and using the non-slip boundary conditions on $z = \pm H/2$ provide the remaining 6 equations that permit to determine the unknowns A , \mathbf{A} , B and \mathbf{B} . In order to proceed as simply as possible, we rewrite the velocity field under the following form:

$$\begin{cases} -\eta v_x(\mathbf{q}, z) = A^x \cosh(qz) + B^x \sinh(qz) - \frac{iq_x}{2q} z A \sinh(qz) - \frac{iq_x}{2q} z B \cosh(qz) - \eta v_x^0(z) \\ -\eta v_y(\mathbf{q}, z) = A^y \cosh(qz) + B^y \sinh(qz) - \frac{iq_y}{2q} z A \sinh(qz) - \frac{iq_y}{2q} z B \cosh(qz) - \eta v_y^0(z) \\ -\eta v_z(\mathbf{q}, z) = A^z \sinh(qz) + B^z \cosh(qz) - \frac{1}{2} A z \cosh(qz) - \frac{1}{2} B z \cosh(qz) - \eta v_z^0(z) \end{cases} \quad (25)$$

with

$$\eta \mathbf{v}^0(z) = \eta \begin{pmatrix} v_x^0(z) \\ v_y^0(z) \\ v_z^0(z) \end{pmatrix} = - \begin{pmatrix} \frac{q_x^2}{4q^2} |z - z_0| + \frac{1}{2q} - \frac{q_x^2}{4q^3} \\ \frac{q_x q_y}{4q^2} |z - z_0| - \frac{q_x q_y}{4q^3} \\ -\frac{iq_x(z - z_0)}{4q} \end{pmatrix} e^{q|z - z_0|} F_{11} \quad (26)$$

By introducing:

$$\mathbf{V}^{(0)+} = \frac{1}{2} [\mathbf{v}^0(H/2) + \mathbf{v}^0(-H/2)] \quad (27)$$

$$\mathbf{V}^{(0)-} = \frac{1}{2} [\mathbf{v}^0(H/2) - \mathbf{v}^0(-H/2)] \quad (28)$$

and exploiting the parity of hyperbolic functions, the six non-slip conditions may be rewritten as:

$$\begin{cases} 0 = A^x \cosh(qH/2) - \frac{iq_x}{2q} \frac{H}{2} A \sinh(qH/2) - \eta V_x^{(0)+} \\ 0 = B^x \sinh(qH/2) - \frac{iq_x}{2q} \frac{H}{2} B \cosh(qH/2) - \eta V_x^{(0)-} \\ 0 = A^y \cosh(qH/2) - \frac{iq_y}{2q} \frac{H}{2} A \sinh(qH/2) - \eta V_y^{(0)+} \\ 0 = B^y \sinh(qH/2) - \frac{iq_y}{2q} \frac{H}{2} B \cosh(qH/2) - \eta V_y^{(0)-} \\ 0 = A^z \sinh(qH/2) - \frac{A}{2} \frac{H}{2} \cosh(qH/2) - \eta V_z^{(0)-} \\ 0 = B^z \cosh(qH/2) - \frac{B}{2} \frac{H}{2} \sinh(qH/2) - \eta V_z^{(0)+} \end{cases} \quad (29)$$

From these relations we express \mathbf{A} and \mathbf{B} as a function of A and B :

$$\mathbf{A} = \begin{pmatrix} \frac{1}{\cosh(qH/2)} [\eta V_x^{(0)+} + \frac{iq_x}{2q} \frac{H}{2} A \sinh(qH/2)] \\ \frac{1}{\cosh(qH/2)} [\eta V_y^{(0)+} + \frac{iq_y}{2q} \frac{H}{2} A \sinh(qH/2)] \\ \frac{1}{\sinh(qH/2)} [\eta V_z^{(0)-} + \frac{A}{2} \frac{H}{2} \cosh(qH/2)] \end{pmatrix} \quad (30)$$

$$\mathbf{B} = \begin{pmatrix} \frac{1}{\sinh(qH/2)} [\eta V_x^{(0)-} + \frac{iq_x}{2q} \frac{H}{2} B \cosh(qH/2)] \\ \frac{1}{\sinh(qH/2)} [\eta V_y^{(0)-} + \frac{iq_y}{2q} \frac{H}{2} B \cosh(qH/2)] \\ \frac{1}{\cosh(qH/2)} [\eta V_z^{(0)+} + \frac{B}{2} \frac{H}{2} \sinh(qH/2)] \end{pmatrix} \quad (31)$$

Finally, inserting these relations in Eq. 23 we obtain the expression of A and B as a function of $\mathbf{V}^{(0)+}$ and $\mathbf{V}^{(0)-}$:

$$\begin{aligned} A &= \frac{2i\eta}{1 - \frac{qH}{\sinh(qH)}} \left[\frac{1}{\cosh(qH/2)} \{q_x V_x^{(0)+} + q_y V_y^{(0)+}\} - \frac{iq}{\sinh(qH/2)} V_z^{(0)-} \right] \\ B &= \frac{2i\eta}{1 + \frac{qH}{\sinh(qH)}} \left[\frac{1}{\sinh(qH/2)} \{q_x V_x^{(0)-} + q_y V_y^{(0)-}\} - \frac{iq}{\cosh(qH/2)} V_z^{(0)+} \right] \end{aligned} \quad (32)$$

Inserting Eq 32 in Eqs 30 and 31, and substituting into Eq 20 provides, after straightforward although tedious calculations, the desired solution for $v_x(\mathbf{q}, z, z_0)$.

The xx component of the mobility tensor $\mathbb{T}^\infty(\mathbf{r}, \mathbf{r}_0)$ then follows as the inverse 2D Fourier transform in the particular case $F_{\parallel} = 1$, and the yy component can be obtained similarly by computing $v_y(\mathbf{q}, z, z_0)$ under a perturbation along the y axis. The parallel component is finally $\mathbb{T}_{\parallel} = \frac{1}{2} (\mathbb{T}_{xx}^\infty + \mathbb{T}_{yy}^\infty)$. The computation of the inverse 2D Fourier transform is difficult, but in fact unnecessary. Indeed, for our purpose we only need to compute averages of the mobility over the pore width. This involves integrals over z and z_0 , as explained in the next section, as well as over x and y which are computed directly from the value of the 2D Fourier transform for $\mathbf{q} = \mathbf{0}$.

Computation of the associated averages along z

As explained in the main text, two different vertical averages must be computed. For the effect of the background $\langle \delta\mathbb{T}^b \rangle$ the average velocity is taken over z and z_0 independently:

$$\hat{f}_{z,z_0}^{xx}(\mathbf{q}) = \frac{1}{H^2} \int_{-H/2}^{H/2} \int_{-H/2}^{H/2} dz dz_0 v_x(\mathbf{q}, z, z_0). \quad (33)$$

Similarly the yy component is obtained by applying the Stokeslet in the y direction and computing v_y . This double integral can be performed using the full solution of section , with the result in tensorial form:

$$\hat{f}_{z,z_0}(\mathbf{q}) = \frac{(\mathbb{1} - \hat{\mathbf{q}}\hat{\mathbf{q}})}{\eta q^2} \frac{1}{H} \left[1 - \frac{\tanh(qH/2)}{qH/2} \right], \quad (34)$$

with $\mathbb{1}$ the 2D identity matrix and $\hat{\mathbf{q}}$ a unit vector in reciprocal space. The parallel component, given by the half-trace of this tensor, is particularly simple:

$$\hat{f}_{z,z_0}(q) = \frac{1}{2\eta q^2 H} \left[1 - \frac{\tanh(qH/2)}{qH/2} \right]. \quad (35)$$

Finally, the integral over $x - x_0$ and $y - y_0$ is obtained as the value of this 2D Fourier transform for $\mathbf{q} = \mathbf{0}$, namely: $\hat{f}_{z,z_0}(0) = H/24\eta$. Combined with the $1/L^2$ factor for the average in Eq. 5 of the main text, this leads to the final result:

$$\langle \delta\mathbb{T}_{\parallel}^b \rangle = \frac{1}{24\eta} \frac{H}{L^2}. \quad (36)$$

For the effect of periodic images $\langle \delta\mathbb{T}^i \rangle$, the average is taken over $z = z_0$, *i.e.*:

$$\hat{f}_{z_0,z_0}(\mathbf{q}) = \frac{1}{H} \int_{-H/2}^{H/2} dz_0 v_x(\mathbf{q}, z_0, z_0). \quad (37)$$

The solution in that case is lengthier. The final result for the half-trace reads:

$$\hat{f}_{z_0,z_0}(q) = \frac{9 + 12q^2H^2 - 2q^4H^4 - 9 \cosh(2qH) - 12q^3H^3 \coth(qH) + 9qH \sinh(2qH)}{48\eta q^2 H [\sinh^2(qH) - q^2H^2]} \quad (38)$$

Here again the value of the integral over $x - x_0$ and $y - y_0$ is obtained as the $\mathbf{q} = \mathbf{0}$ value of this 2D Fourier transform, namely:

$$\hat{f}_{z_0,z_0}(0) = \frac{7H}{60\eta}. \quad (39)$$

III. Asymptotic results

As explained in the main text, the correction to the diffusion coefficient due to periodic boundary conditions is given by $\Delta D_{\parallel} = k_B T \left[\langle \delta T_{\parallel}^i \rangle - \langle \delta T_{\parallel}^b \rangle \right]$, where we have already computed the background correction $\langle \delta T_{\parallel}^b \rangle$ in Eq. 36. Here we derive asymptotic expressions in the regimes of elongated and flat systems for the effect of periodic images:

$$\langle \delta T_{\parallel}^i \rangle = \frac{1}{H} \int_0^H dz \sum_{(m,n) \neq (0,0)} T_{\parallel}^{\infty}(-mL, -nL, z, z). \quad (40)$$

Elongated systems ($H \gg L$)

For elongated systems, we can approximate the discrete sum in Eq. 40 by an integral, provided that we remove the contribution corresponding to $(m, n) = (0, 0)$ which is not included in the sum:

$$\begin{aligned} \sum_{(m,n) \neq (0,0)} T_{\parallel}^{\infty}(-mL, -nL, z, z) &\approx \iint_{-\infty}^{\infty} \frac{dx_0 dy_0}{L^2} T_{\parallel}^{\infty}(-x_0, -y_0, z, z) \\ &\quad - \iint_{-L/2}^{L/2} \frac{dx_0 dy_0}{L^2} T_{\parallel}^{\infty}(-x_0, -y_0, z, z). \end{aligned} \quad (41)$$

The first integral is computed easily using the results of the previous section. From Eq. 39, one readily obtains for the average over z :

$$\frac{1}{H} \int_0^H dz \iint_{-\infty}^{\infty} \frac{dx_0 dy_0}{L^2} T_{\parallel}^{\infty}(-x_0, -y_0, z, z) = \frac{1}{L^2} \hat{f}_{z_0, z_0}(0) = \frac{7}{60\eta} \frac{H}{L^2}. \quad (42)$$

The second integral can be rewritten as a convolution between T_{\parallel}^{∞} and a rectangular function with value 1 if $(x_0, y_0) \in [-\frac{L}{2}, \frac{L}{2}] \times [-\frac{L}{2}, \frac{L}{2}]$ and zero otherwise. This convolution product is conveniently computed in Fourier space, using the result Eq. 38 and the well-known transform of the rectangular function. The average over z then reads:

$$\begin{aligned} \langle \delta T_{\parallel}^{\text{self}} \rangle &= \frac{1}{H} \int_0^H dz \iint_{-L/2}^{L/2} \frac{dx_0 dy_0}{L^2} T_{\parallel}^{\infty}(-x_0, -y_0, z, z) \\ &= \frac{1}{4\pi^2 \eta} \iint_{-\infty}^{\infty} dq_x dq_y \hat{f}_{z_0, z_0}(q) \frac{\sin(q_x L/2)}{q_x L/2} \frac{\sin(q_y L/2)}{q_y L/2}, \end{aligned} \quad (43)$$

with $\hat{f}_{z_0, z_0}(q)$ given by Eq. 38 and $q = \sqrt{q_x^2 + q_y^2}$. We first make a change of variables, $u_x = q_x L$ and $u_y = q_y L$:

$$\langle \delta T_{\parallel}^{\text{self}} \rangle = \frac{1}{4\pi^2 L^2} \iint_{-\infty}^{\infty} du_x du_y \hat{f}_{z_0, z_0}\left(\frac{u}{L}\right) \frac{\sin(u_x/2)}{u_x/2} \frac{\sin(u_y/2)}{u_y/2}, \quad (44)$$

with $u = \sqrt{u_x^2 + u_y^2}$. Now, the regime of elongated boxes corresponds to $H/L \rightarrow \infty$, so that we can approximate $\hat{f}_{z_0, z_0}(\frac{u}{L})$ by the asymptotic expansion of $\hat{f}_{z_0, z_0}(q)$ for $q \rightarrow \infty$, namely:

$$\hat{f}_{z_0, z_0}(q \rightarrow \infty) \approx \frac{3}{8\eta q}, \quad (45)$$

which can be derived from the full expression Eq. 38. Inserting this approximation into Eq. 46, we obtain:

$$\langle \delta T_{\parallel}^{\text{self}} \rangle \approx \frac{1}{\pi^2 L^2} \frac{3L}{8\eta} \iint_{-\infty}^{\infty} du_x du_y \frac{1}{\sqrt{u_x^2 + u_y^2}} \frac{\sin(u_x/2)}{u_x} \frac{\sin(u_y/2)}{u_y} = \frac{3}{8\pi^2 \eta L} \times I. \quad (46)$$

The integral I defined by the second equality can be computed analytically by writing:

$$\frac{1}{\sqrt{u_x^2 + u_y^2}} = \frac{1}{\sqrt{\pi}} \int_{-\infty}^{\infty} dt e^{-t^2(u_x^2 + u_y^2)}. \quad (47)$$

We then rewrite:

$$\begin{aligned}
I &= \frac{1}{\sqrt{\pi}} \int_{-\infty}^{\infty} dt \iint_{-\infty}^{\infty} du_x du_y e^{-t^2(u_x^2+u_y^2)} \frac{\sin(u_x/2)}{u_x} \frac{\sin(u_y/2)}{u_y} \\
&= \frac{1}{\sqrt{\pi}} \int_{-\infty}^{\infty} dt \left[\int_{-\infty}^{\infty} du e^{-t^2 u^2} \frac{\sin(u/2)}{u} \right]^2 \\
&= \frac{1}{\sqrt{\pi}} \int_{-\infty}^{\infty} dt \left[\pi \operatorname{erf} \left(\frac{1}{4t} \right) \right]^2 = 2\pi \ln(1 + \sqrt{2}) .
\end{aligned} \tag{48}$$

In the last line we have introduced the error function and computed the remaining integral analytically. Gathering the result with Eq. 46, we obtain $\langle \delta T_{\parallel}^{\text{self}} \rangle = 3 \ln(1 + \sqrt{2})/4\pi\eta L$, which, together, with Eqs. 40, 41 and 42 provides:

$$\langle \delta T_{\parallel}^i \rangle = \frac{7}{60\eta} \frac{H}{L^2} - \frac{3 \ln(1 + \sqrt{2})}{4\pi\eta L} . \tag{49}$$

Finally, the complete solution for the correction to the diffusion coefficient is obtained by subtracting the contribution of the background, Eq. 36:

$$\Delta D_{\parallel}(H > L) = k_B T \left[\langle \delta T_{\parallel}^i \rangle - \langle \delta T_{\parallel}^b \rangle \right] = \frac{k_B T}{\eta} \left[\frac{3}{40} \frac{H}{L^2} - \frac{3 \ln(1 + \sqrt{2})}{4\pi L} \right] , \tag{50}$$

which is Eq. 6 of the main text.

Flat systems ($L \gg H$)

Here we show that the mobility tensor T_{\parallel}^{∞} decays exponentially fast with distance in real space, so that the interaction between periodic images $\langle \delta T_{\parallel}^i \rangle$ is negligible compared to the effect of the background $-\langle \delta T_{\parallel}^b \rangle$. To that end, we need to compute the inverse Fourier transform of $\hat{f}_{z_0, z_0}(q)$:

$$\hat{f}_{z_0, z_0}(r) = \frac{1}{2\pi} \int_0^{\infty} dq q J_0(qr) \hat{f}_{z_0, z_0}(q) \tag{51}$$

where $\hat{f}_{z_0, z_0}(q)$ is given by Eq. 38 and J_0 is the zeroth-order Bessel function of the first kind. This calculation is much more involved than the previous ones, which only required the $q \rightarrow 0$ and $q \rightarrow \infty$ limits of $\hat{f}_{z_0, z_0}(q)$. Liron and Mochon [2] evaluated such integrals using the Hankel contour illustrated in Figure 4. The real-space function is

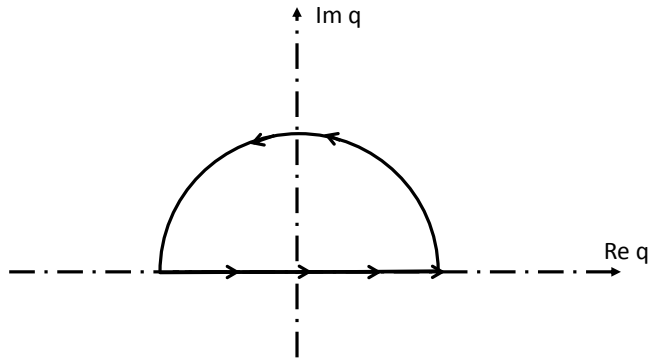


FIG. 4. The integration contour in the complex q -plane

then given by:

$$\hat{f}_{z_0, z_0}(r) = \operatorname{Re} \left(\frac{i}{2} \times \text{sum of residues in upper half plane of } \hat{f}_{z_0, z_0}(q) q H_0^{(1)}(qr) \right) \tag{52}$$

where the function $\hat{f}_{z_0, z_0}(q)$ given by Eq. 38 is now understood as a function of the complex variable q and is itself complex valued. The function $H_0^{(1)}$ is a Hankel function given by $H_0^{(1)}(z) = J_0(z) + iY_0(z)$, with Y_0 the zeroth-order Bessel function of the second kind. The function $\hat{f}_{z_0, z_0}(q)qH_0^{(1)}(qr)$ has no pole at the origin, but an infinite number of poles corresponding to the coth function (except at the origin) and additional poles denoted s_n corresponding to the solutions of the transcendental equation $\sinh(s)^2 = s^2$. For large n the asymptotic behavior of these poles is given by:

$$s_n = x_n + iy_n \simeq \ln(2n + 1)\pi + i(n + 1/2)\pi. \quad (53)$$

The net result appears as an absolutely convergent series of functions involving modified Bessel functions $K_0(n\pi r/H) \propto \sqrt{\frac{H}{r}} \exp(-n\pi r/H)$ coming from the residues arising from the coth function. An additional series of Bessel functions $|H_0^{(1)}(s_n r/H)| \propto \frac{\pi}{2} \sqrt{\frac{H}{r}} \exp(-y_n r/H)$ comes from the residues associated with the s_n poles. As in both cases, the imaginary part of the poles behaves as an arithmetic sequence, the associated series can be approximated by their first term for large r/H . Overall, the asymptotic behavior for large r/H is given by:

$$\hat{f}_{z_0, z_0}(r) \sim \sqrt{\frac{H}{r}} \exp(-\pi r/H), \quad (54)$$

i.e. an exponentially decreasing correction. This result can in fact be recovered using equation (49) of Liron and Mochon [2], by computing the required trace that suppresses the long-range contribution, and performing the associated $\hat{E}(z_0, z_0)$ average term by term in the resulting series. The exponential decay in real space implies that the sum over periodic images is dominated for flat systems ($L \gg H$) by the nearest images, so that this sum also decays exponentially fast with L/H . Overall, confinement screens the hydrodynamic interactions between the periodic images and the corresponding contribution $\langle \delta T_{\parallel}^i \rangle$ is negligible compared to the effect of the background $-\langle \delta T_{\parallel}^b \rangle$.

-
- [1] A. Saugey, L. Joly, C. Ybert, J. L. Barrat, and L. Bocquet, *Journal of Physics: Condensed Matter* **17**, S4075 (2005).
 - [2] N. Liron and S. Mochon, *Journal of Engineering Mathematics* **10**, 287 (1975).
 - [3] J. W. Swan and J. F. Brady, *Physics of Fluids* (1994-present) **22**, 103301 (2010).